THz Letters

Low-Frequency Noise and Passive Imaging With 670 GHz HEMT Low-Noise Amplifiers

Erich N. Grossman, *Senior Member, IEEE*, Kevin Leong, Xiaobing Mei, and William Deal, *Member, IEEE*

***Abstract*—We combine newly developed InP HEMT amplifiers operating at 670 GHz with a zero-bias diode (ZBD) in order to investigate limits on passive imaging performance possible with fully uncooled, direct-detection technology. Noise-equivalent temperature difference (NETD) values under 2 K are found for reference conditions (30 Hz modulation). However, noise spectra continue to fall approximately as $1/f$ out to "knee" frequencies of several hundred hertz (Hz) and spectral densities of $\sim$0.12 K/Hz$^{1/2}$ for the current, somewhat gain-starved, amplifiers. The amplifier alone contributes 0.043 K/Hz$^{1/2}$. These results indicate that modest-sized, rapidly scanned arrays should provide real-time, passive imaging—desired for standoff security screening and other applications—with the same image quality as cryogenic bolometer arrays.**

***Index Terms*—Imaging, passive, submillimeter (submm), terahertz (THz), $1/f$-noise, HEMT, InP.**

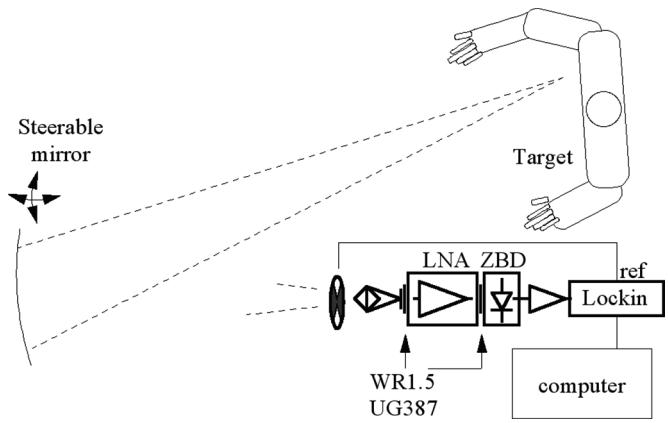

Fig. 1. Experimental setup, as configured for imaging a human figure at a range of $\sim$1.2 m.

I. Introduction

THE recent development of transistors and monolithic integrated circuits operating at submillimeter-wave (submm) frequencies (300 GHz and above) can enable uncooled systems to fulfill measurement needs that previously required cryogenic devices. In particular, the latest generation of InP HEMT transistors [1] and HBT transistors [2], [3] have been developed with active imaging radar applications in mind [4]. Imaging radars operating as high as 650 GHz [5] are now being adapted to exploit them. *Passive* submm imaging on the other hand, has primarily been addressed with cryogenic sensor arrays [6]–[11]. The present work demonstrates that the new generation of HEMT amplifiers does indeed provide adequate sensitivity for passive submm imaging in terrestrial (indoor or outdoor) applications.

Similar work has been carried out at lower frequencies, including an uncooled real-time imager operating at 250 GHz that is now a commercial product [12]. Earlier, the U.S. DARPA's MIATA program [13] also notably resulted in uncooled zero-bias diode arrays for the 100–200 GHz band whose noise-equivalent temperature difference (NETD) approached 2 K. Though not quite sensitive enough to use alone for indoor real-time imaging, it was found [14] that those detectors could be combined with low-noise amplifiers in a small module that provided NETD $<$ 0.5 K. A key issue for such modules is low-frequency noise, from both the zero-bias diode (which is not at exactly zero bias in operation) and the high-frequency amplifier. The present work takes the same basic approach, combining a high-frequency, but relatively low gain, low-noise amplifier (LNA) with a sensitive zero-bias diode. A fully comprehensive description of this module's performance, comparable to [14], is beyond the scope of this letter. However, the newness of the submm HEMT technology and its high potential impact, justifies a "first look" at the $1/f$ noise and other performance-limiting questions that apply to passive submm imaging, whether for security screening, atmospheric remote sensing, or other applications. While the optimal frequency is different for each application, 670 GHz is significant as the current limit of high frequency transistor technology.

II. Measurements

The basic experimental setup is illustrated in Fig. 1. The packaged low-noise amplifiers (LNAs), designed and fabricated at Northrop-Grumann, are described in [15]. Two separate units were included in this study, denoted 2-1 and 2-2, the latter displaying significantly lower gain ($\sim$3 dB) than the former in separate S-parameter measurements (not shown).

Manuscript received March 31, 2014; revised June 12, 2014; accepted August 07, 2014. Date of production September 04, 2014; date of current version October 30, 2014. This work was supported by the U.S. Defense Advanced Research Projects Agency (DARPA) under the Terahertz Electronics program.

E. N. Grossman is with the National Institute of Standards and Technology, Boulder, CO 80305 USA (e-mail: erich.grossman@nist.gov).

K. Leong, X. Mei, and W. Deal are with Northrop Grumman Corporation, Redondo Beach, CA 90278 USA.

Color versions of one or more of the figures in this paper are available online at http://ieeexplore.ieee.org.

Digital Object Identifier 10.1109/TTHZ.2014.2352035

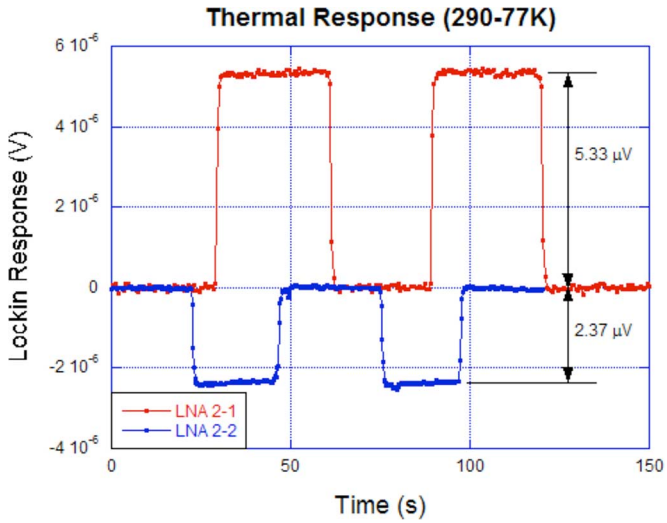

Fig. 2. Response to radiometric loads at 77 K. Phase has been reversed for one of the units, for clarity.

The ZBD is a commercial unit, with a measured zero-bias resistance of $R_0 = 1.75$ kΩ and nominal responsivity of 750 V/W, (referred to the input flange). Both ZBD and LNA are packaged in WR-1.5 rectangular waveguide blocks, with standard UG-387 flanges at input and output. The low-frequency (video) output of the ZBD is fed to a low-noise (gain = 100, 1.4 nV/Hz$^{1/2}$) bipolar preamp, and thence to a lockin amplifier for imaging or radiometric (thermal) responsivity measurements, or to an audio spectrum analyzer for low-frequency noise measurements. No Dicke switch is included in the LNA input, so simple optical chopping, at 50 Hz, is used to modulate the input signal and partially cancel radiometric drifts and offsets. A significant, but easily eliminated, artifact is introduced by the LNA's imperfect input match (S_{11}), when the chopper blade is aligned at particular orientations, where emission from the waveguide is coupled back into it. The antenna is a commercial, WR1.5 pyramidal horn with 3.63×2.77 mm entrance aperture, nominal gain of 25 dB, and 90% encircled beam radius (in the far field) of 10°. It should be noted that the intrinsic passband of the LNA (see, for example, on-wafer measurements in [1]), as well as the passband defined by the ZBD, combine to provide a very sharp cutoff to the module's high-frequency response. In contrast to bolometric approaches, external low-pass filters are unnecessary for passive imaging with transistor circuits.

A. Radiometric Responsivity

Radiometric responsivity was measured simply by placing loads of submm absorber material (Emerson-and Cuming, AN-72) cooled to liquid nitrogen (LN2) temperature in a Styrofoam container, directly in the antenna beam, immediately after the chopper. The loads were substantially oversized, to ensure the entire beam was terminated at T = 77 K. The raw lockin output is shown in Fig. 2. This is converted to the module's radiometric responsivity using

$$\frac{dV}{dT} = \frac{\pi}{\sqrt{2}} \frac{V_{\text{lockin}}}{\Delta T}. \quad (1)$$

TABLE I

	LNA 2-1	LNA 2-2
Drain, Gate Bias (V)	1.30, 0.22	1.30, 0.24
Bias current (mA)	66	71
Thermal Responsivity (nV/K)	55.6	24.7
V_{DC} (μV)	535	276
T_{sys} (K)	9,600	11,200
$\sqrt{S_w'}$ (nV/Hz$^{1/2}$)	5.96	6.04
$\sqrt{S_w}$ (nV/Hz$^{1/2}$)	2.41	2.82
Noise BW (GHz)	98	19
Reference NETD (K)	1.8	1.9

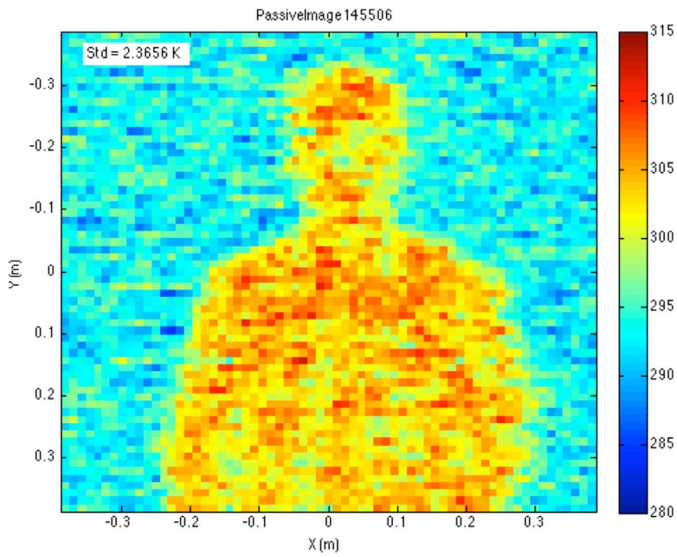

Fig. 3. Passive 4.2 kpixel image of one of the authors taken with LNA2-1, and raster-scanned as described in the text. Z-axis is radiometric temperature in kelvin (K).

The factor of $\pi/\sqrt{2}$ arises from standard lockin calibration; using $\Delta T = 213$ K yields the responsivity values in Table I.

B. Imaging

Radiometric responsivities in the 20–50 nV/K range suggest that, with careful attention to low-noise techniques, high quality images can be obtained from targets with internal temperature contrasts of order 1 K, typical of indoor scenes. A substantial number of such passive images have been acquired by raster-scanning the primary mirror as shown in Fig. 1. Targets include human figures against a large plywood background—see Fig. 3 for a representative example—and NIST's Aqueous Blackbody Calibration (ABC) source [16] against a (cluttered) laboratory background. The latter's design is optimized for 200–400 GHz however, so its accuracy at 650 GHz is not necessarily any better than the LN2-cooled absorber that was actually used for the calibration. The mirror is a 30 cm diameter, 1 m focal length (50 cm radius of curvature) spherical aluminum mirror. Nominal distance from horn aperture to mirror vertex was 68 cm, distance from vertex to nominal target plane, 1.2 m. Use of a spherical mirror off-axis does introduce a certain amount of astigmatism. Prior submm imaging experiments (using cryogenic bolometers) have shown this issue to be minor.

The radiometric temperature scale was calibrated by placing the LN2-cooled absorber in the target plane and repeating the measurement of Section II-A. This indicated an aperture efficiency for the primary mirror of 65%, somewhat lower than the 90% expected from the feedhorn beam and the optical configuration. Each pixel in the 65×65 image shown in Fig. 3 covered a 12.0×12.0 mm area and used an integration time of 300 ms per pixel. The indicated per-pixel standard deviation of 2.4 K was evaluated simply from the upper left 19×19 cm corner of the image. It therefore includes fluctuations unrelated to the module's noise, including real variations in background temperature, electromagnetic interference, etc. Although this clearly indicates that the module's noise performance is potentially promising for uncooled imaging of indoor scenes, a rigorous evaluation requires measurement of its noise power spectral density (PSD).

C. Low-Frequency Noise

For noise measurements, the (unchopped) feedhorn beam was terminated in room temperature absorber. The top panel of Fig. 4 displays voltage noise spectra from the module for each of the two LNA's, the spectrum produced by the ZBD alone (i.e., with LNA turned off), and the spectrum produced by the audio frequency amplifier alone (input shorted), along with fits to each spectrum.

The PSD spectra consist of white noise $\mathrm{S_w}$ combined with a low-frequency component that is well-approximated by a 1/f spectrum, $\mathrm{S_1/f}$. The "knee" frequency, where the two components contribute equally, lies at 500 and 100 Hz for LNA2-1, and LNA2-2 respectively. The white noise is dominated by Johnson noise of the ZBD, $\sqrt{4kT_0R_0} = 5.4$ nV/Hz$^{1/2}$. However, it displays a small but significant increase, when the LNA is turned on. The ZBD also produces a small DC voltage $\mathrm{V_{DC}}$ when the LNA is turned on, due to rectification of the LNA's amplified input noise, integrated over its bandwidth. As described in [14, eqns. (11), (36)], the LNA-induced white noise, $\mathrm{V_{DC}}$, and the LNA bandwidth are related by

$$\mathrm{BW} = \frac{2V_{\mathrm{DC}}^2}{S_w}$$

where

$$S_w = S_w^{'} - 4kTR_0 \tag{2}$$

and where $S_w^{'}$ is the total white noise. Moreover, $\mathrm{V_{DC}}$ defines an "equivalent system temperature" via $T_{\mathrm{sys}} = (V_{\mathrm{DC}})/(dV/dT)$. $\mathrm{V_{DC}}$ constitutes an effective "self-bias" on the ZBD and introduces the possibility of $1/f$ noise, analogous to that seen in biased Schottky diodes. Values for all parameters, measured independently for the two LNA units, are given in Table I.

The low frequency component is dominated by noise that disappears when the LNA is turned off. At 50 Hz, where the image of Fig. 3 was acquired, this component is dominant. Though superficially LNA2-1 displays significantly higher $1/f$-noise than LNA2-2, this is merely a result of its higher gain, like its higher radiometric responsivity and $\mathrm{V_{DC}}$. When referred to radiometric temperature at the input, the two units display the same level of $1/f$-noise, within the uncertainty. The $1/f$ noise arises from two sources, gain fluctuations in the LNA, and $1/f$ noise in the ZBD. These cannot be separated with the present suite of measurements.

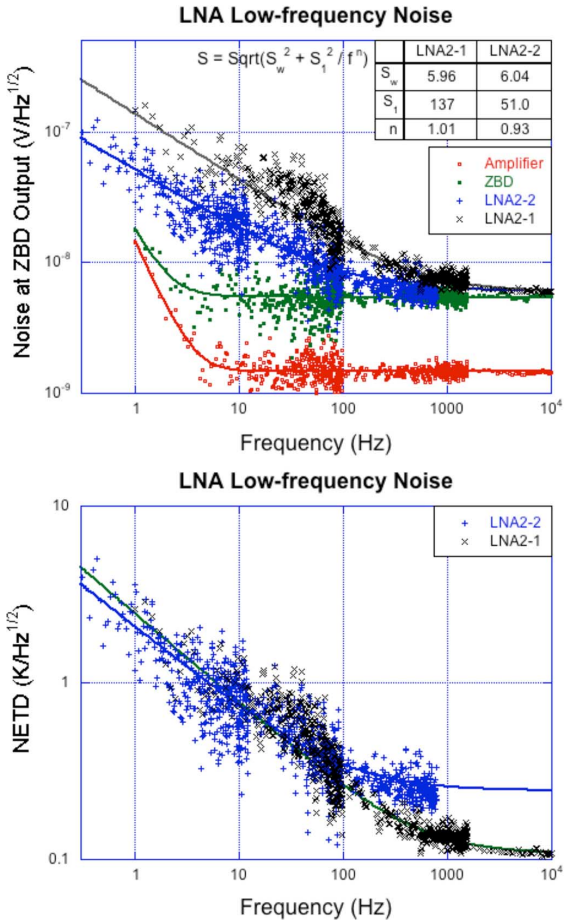

Fig. 4. Noise spectra. The upper panel displays voltage noise referred to the ZBD output. The lower panel displays the same data for the LNAs, but referred to radiometric temperature at the horn input.

III. Discussion and Conclusion

The noise spectrum, referred to radiometric input temperature, yields the NETD spectrum. To avoid ambiguity about time constants, it is conventional for purposes of device comparison to define a "reference" NETD, corresponding to the value of the NETD spectrum at 30 Hz and an unapodized integration time of $\tau = 1/30$ s, i.e.,

$$\mathrm{NETD_{ref}} = \frac{\mathrm{NETD}(f = 30\ \mathrm{Hz})}{\sqrt{2(\tau = 1/30\ \mathrm{s})}}. \tag{3}$$

This figure-of-merit comes out slightly below 2 K for both units. The figures listed in Table I allow us to project the performance of LNAs with slightly higher gain, whose RF noise would dominate ZBD Johnson noise: a white noise floor of $\sqrt{S_w}/(dV/dT) = 0.043$ K/Hz$^{1/2}$, achieved above a knee frequency of 3.4 kHz. The latter corresponds to the sampling frequency in a 10 frame/s imager with 340 samples/frame, typical for current scanned cryogenic sensor arrays. For passive imaging, the combination of HEMT LNA and sensitive ZBD thus provides a viable alternative to cryogenic sensor arrays, offering vastly superior size, weight, and power.

ACKNOWLEDGMENT

The views expressed are those of the authors and do not reflect the official policies or position of the Department of Defense or the U.S. Government. Approved for public release, distribution unlimited.

REFERENCES

[1] W. Deal *et al.*, "THz monolithic integrated circuits using InP high electron mobility transistors," *IEEE Trans. THz Sci. Technol.*, vol. 1, no. 1, pp. 25–32, Sep. 2011.

[2] M. J. W. Rodwell, M. Le, and B. Brar, "InP bipolar ICs: Scaling, roadmaps, frequency limits, manufacturable technologies," *Proc. IEEE*, vol. 96, no. 2, pp. 271–286, Feb. 2008.

[3] M. J. W. Rodwell *et al.*, "THz indium phosphide bipolar transistor technology," in *Proc. Compound Semicond. Symp.*, 2012, pp. 1–4.

[4] H. B. Wallace, "Analysis of RF imaging applications at frequencies over 100 GHz," *Appl. Opt.*, vol. 49, pp. E38–E47, 2010.

[5] K. B. Cooper *et al.*, "Terahertz imaging radar for standoff personnel screening," *IEEE Trans. THz Sci. Technol.*, vol. 1, no. 1, pp. 169–182, Sep. 2011.

[6] E. N. Grossman *et al.*, "Passive terahertz camera for standoff security screening," *Appl. Opt.*, vol. 49, pp. E106–E120, 2010.

[7] A. Luukanen, M. Gronholm, M. Leivo, H. Toivanen, and A. Rautiainen, "Measured performance of a high-resolution passive video-rate submillimeter-wave imaging system demonstrator for standoff imaging," in *Proc. SPIE*, 2012, vol. 8362, pp. 836209–1.

[8] E. Heinz *et al.*, "Passive submillimeter-wave standoff video camera for security applications," *J. Infrared Millim. THz Waves*, vol. 31, pp. 1355–1369, 2010.

[9] D. Becker *et al.*, "High-resolution passive video-rate imaging at 350 GHz," in *Proc. SPIE*, 2011, vol. 8022, pp. 802206-1–802206-9.

[10] S. Ariyoshi *et al.*, "Terahertz imaging with a direct detector based on superconducting tunnel junctions," *Appl. Phys. Lett.*, vol. 88, 2006.

[11] R. V. Ozhegov, K. N. Gorshkov, G. N. Gol'tsman, N. V. Kinev, and V. P. Koshelets, "The stability of a terahertz receiver based on a superconducting integrated receiver," *Supercond. Sci. Technol.*, vol. 24, pp. 1–4, 2011.

[12] T. n. D. Barriers, 2014 [Online]. Available: http://www.digitalbarriers.com/thruvision-ts5/

[13] C. M. Stickley and M. Filipkowski, "Microantenna arrays: Technology and applications; MIATA an overview," in *Proc. 1st Eur. Symp. on Opt. Photon. in Security and Defence*, 2004.

[14] J. J. Lynch *et al.*, "Passive millimeter-wave imaging module with preamplified zero-bias detection," *IEEE Trans. Microw. Theory Techn.*, vol. 56, no. 7, pp. 1592–1600, Jul. 2008.

[15] W. R. Deal *et al.*, "Low noise amplification at 0.67 THz using 30 nm InP HEMTs," *IEEE Microw. Wireless Compon. Lett.*, vol. 21, no. 7, pp. 368–370, Jul. 2011.

[16] C. R. Dietlein, Z. Popovic, and E. N. Grossman, "Aqueous blackbody calibration source for millimeter-wave/terahertz metrology," *Appl. Opt.*, vol. 47, pp. 5604–5615, 2008.